Materials Science & Engineering C 100 (2019) 514–522

Contents lists available at ScienceDirect

Materials Science & Engineering C

journal homepage: www.elsevier.com/locate/msec

Dual-functional core-shell electrospun mats with precisely controlled release of anti-inflammatory and anti-bacterial agents

Shihao Wen, Yupeng Hu, Yuanzhong Zhang, Shifeng Huang, Yuchen Zuo, Younjin Min*

Department of Polymer Engineering, University of Akron, Akron, OH 44325, USA

ARTICLE INFO

Keywords:
Core/shell nanofibers
Wound healing
Silk
β-Sheets
Inflammation
Infection
Flurbiprofen
Vancomycin

ABSTRACT

Acute wounds are worldwide problems affecting millions of people and causing heavy economic burden to national healthcare systems. Herein, we describe novel wound dressing materials relying on core/shell electrospun mats incorporated with flurbiprofen and vancomycin for achieving programmable release of anti-inflammatory and anti-bacterial agents. The shell matrix of nanofibers consisted of polyethylene oxide while the core matrix was made from a blend of silk and collagen. Several optimal mat architectures were engineered with distinct configurations, of which release profiles displayed an exponential trend, which indicates a first-order process following Fickian diffusion behavior. The flurbiprofen release lasted from 2 to 6 days, which was much faster compared to the one of vancomycin prolonged up to about 20 days. Mechanical data indicated tensile modulus, tensile strength, elongation before break of core/shell electrospun mats became enhanced or comparable to those for human skin after methanol vapor treatment. Desirable release kinetics and mechanical characteristics achieved by novel core/shell electrospun mats were attributable to induced enrichment of β-sheet phase in silk via methanol vapor treatment as well as water annealing process with time and judicious selections for matrix materials and mat configurations. The design principles considered in this study successfully addressed a range of inflammation and infection requirements in wound healing, potentially guiding construction of other biomedical coatings and devices.

1. Introduction

Medically, a wound is defined as a disruption in the integrity of the epithelial lining of the skin or mucosa due to physical or thermal damage [1]. Depending on the duration and nature of healing process, the wound is sub-divided into two categories i.e., acute and chronic ones [2]. An acute wound is an injury to the skin caused by an accident or surgical procedure [3]. About 11 million people are affected by acute wounds per annum while about 300,000 people are hospitalized in the United States [4,5]. Acute wounds typically heal in a time-dependent but predictable and concerted fashion of repair with synergistic contributions from platelets, keratinocytes, immune surveillance cells, microvascular cells, and fibroblasts for the restoration of skin damage [6]. There are four critical phases of the wound healing occurring with different time spans: hemostasis and coagulation with a timescale of seconds to hours, inflammation with a time scale of hours to days, proliferation and repair with a time scale of days to weeks, and remodeling leading to scar formation phase with a time scale of weeks to months [7–10]. In contrast to an acute wound, a chronic wound persists over unpredictable amount of time and does not follow typical phases of wound healing [11]. According to the Wound Healing Society, chronic wounds can be categorized into four, i.e., pressure ulcers, diabetic ulcers, venous ulcers and arterial insufficiency ulcers, all of which are characterized by one or more persistent inflammatory stimuli in the early stage of wound healing [12].

Various types of materials have been used as wound dressing, including gauze, hydrogels, foams, and hydrocolloids. While gauzes are the simplest and most commonly used wound dressings, they suffer from high adherence to wound bed, which can detach granulation tissue and cause pain upon removal [13,14]. In addition, non-degrading fibers of gauzes may be left in the wound, causing inflammation and adversely influencing the healing time [15–17]. Also, woven gauzes are very permeable, which may result in the desiccation of wounds [18–20]. Hydrogel dressings contain three-dimensional network of hydrophilic polymers such as sodium alginate, chitosan, dextran, hydroxyethyl starch, glucan, hyaluronic acid, poly-*N*-acetylglucosamine, and gelatin [21]. While their key benefits are high exudates capacity, non-adherence, and pain and inflammatory reduction, their permeable nature makes them inefficient bacterial barriers and also sometimes poor mechanical stability and leakage can be an issue with hydrogel

* Corresponding author.
E-mail address: ymin@uakron.edu (Y. Min).

https://doi.org/10.1016/j.msec.2019.02.076
Received 16 September 2018; Received in revised form 6 February 2019; Accepted 20 February 2019
Available online 23 February 2019
0928-4931/

dressings [22,23]. Foam dressings, which are mostly made from polyurethane or polysiloxane, tend to be highly absorbent, keep wound area moist, and contains bacterial barrier layer on the backside [24]. However, they are likely to affix to wound bed strongly. In hydrocolloid dressings, a combination of gelatin, pectin, elastomers, and/or sodium carboxymethylcellulose are attached to an adhesive matrix to form a material with non-adherent characteristics and high absorbency [25,26]. Their limitations include unpredictable bacterial barrier properties, high volumes of exudate leakage, and impermeable to gas transport [25,26].

To overcome the challenges of traditional wound dressings, enormous amount of research has been ongoing and various types of novel materials have been described in the literature [27–39]. Among various strategies, electrospun materials have been shown to be especially suitable for wound healing applications because nanofibers produced via the electrospinning process give rise to a highly porous material with a high surface-to-volume ratio that ensures a sufficient gas permeation. These characteristics facilitate cell respiration, moisture retention, remove of exudates, and hemostasis [40]. Furthermore, it is possible to load therapeutic or antibacterial agents into the nanofibers to produce functional mats for more effective wound healing. For example, Kim and co-workers relied on the electrospinning of polyurethane, cellulose acetate, zein, and streptomycin sulfate (antibacterial agent) to prepare nanofibrous composite mats for wound dressing [41]. Zheng et al. dispersed nano-hydroxyapatite containing amoxicillin in poly(lactic-*co*-glycolic acid) to produce a composite antibacterial electrospun wound dressing [42]. Uyar and co-workers reported mats involving nanofibers made from a mixture of hydroxypropyl-beta-cyclodextrin and hydroxypropyl-gamma-cyclodextrin loaded with triclosan [43]. Montazer and Malekzadeh demonstrated the feasibility of production of nylon nanofibers containing silver nanoparticles, which were formed by the reduction of silver nitrate in the polymer solution, via electrospinning [44]. These fibers resulted in 98% to 100% reduction in *Escherichia coli* and *Staphylococcus aureus* growth. Schneider et al. [45] reported that epidermal growth factor can be loaded into the electrospun silk mats and the resultant dressing can achieve slowly release characteristics with 25% EGF release in one week upon contacting the wound. However, these previously developed materials for wound healing have limited tunability to effectively address a sequence of time-dependent wound healing events at different stages, e.g., to better alleviate inflammation response and subsequently prevent bacterial infection on the wound site.

Herein, we report the preparation and characterization of electrospun core-shell nanofiber mats incorporated with two small therapeutic agents, flurbiprofen and vancomycin, to synergistically combat both inflammation and infection in a timely fashion. Flurbiprofen is non-steroidal anti-inflammatory drug that reduces the activity of cyclooxygenase, thereby inhibiting arachidonic acid metabolism and prostaglandin production [46]. The release of flurbiprofen was enhanced by localizing it into the hydrophilic shell (polyethylene oxide) of core/shell nanofibers so that it can reach the minimum effective dosage (10 mg/mL, [47]) within a few hours and maintain these concentration levels for several days. Vancomycin is a potent antibiotic agent with a minimum inhibitory concentration of 2 μg/mL [48]. Considering the bacterial infections can hinder healing mostly before mid/late proliferation phase, we introduced silk protein polymers which are rich with β-sheet structures aiming to slow down and prolong the release up to 20 days. The time-evolved changes on structural, mechanical, and thermal properties of the developed electrospun mats were also identified to assess their suitability as advanced wound healing materials.

2. Materials and methods

2.1. Materials

Cocoons of *Bombyx mori* silkworm silk were purchased from Aurora Silk, Co. (Portland, OR). Cocoons with similar size and clean appearance were selected to be used in the experiments. The type I collagen (300,000 g/mol), which was derived from calf skin, was procured from DSM, Co. (Exton, PA). Sodium carbonate (Na_2CO_3, 99.9%), lithium bromide (LiBr, 99.9%), flurbiprofen, vancomycin hydrochloride hydrate, and polyethylene oxide (PEO, average molecular weight of 900,000 g/mol) were purchased from Sigma-Aldrich (St. Louis, MO).

2.2. Preparation of silk fibroin solution

Silk fibroin solution was prepared as described Rockwood et al. [49]. Cocoons were boiled for 30 min in an aqueous solution of 0.02 M Na_2CO_3 and then rinsed thoroughly with water to extract the sericin proteins. The extracted silk was then dissolved in 9.3 M LiBr solution at 60 °C for 4 h. Afterwards, the yielded solution was dialyzed in water using a dialysis cassette (Slide-a-Lyzer, MWCO 3500, Thermo Scientific). Then, the dialysate was centrifuged at 4 °C and 4000 rpm for 20 min twice. The supernatant was collected, analyzed gravimetrically to determine silk content, and stored at 4 °C until use.

2.3. Preparation of electrospinning solutions

The sheath (shell) part of electrospinning solution involved PEO (3.0 wt%), which was prepared by homogenously dispersing PEO in milli-Q water using rotatory mixing for 24 h at room temperature. Then, 50 mg flurbiprofen was dissolved in 1 mL ethanol, which was later mixed with the PEO solution at a 1:400 (ethanol:water) volume ratio to obtain the shell part of the electrospinning solution. For the core part of electrospinning solution, first, 12 mg type I collagen was dispersed in 0.3 mL milli-Q water at 60 °C for 30 min. Then, 2.85 mL silk solution (8.0 wt%) and 0.5 mL PEO solution (3.0 wt%) was added to the collagen solution at room temperature and homogenized with a rotatory mixer for 3 h. The final weight ratio among the three components for the core electrospinning solution was 5:6:89 for collagen, PEO, and silk, respectively. Then, vancomycin was dissolved in the electrospinning solution containing collagen, PEO, and silk at a concentration of 1.7 wt%.

2.4. Preparation of core-shell nanofibers

After preparing electrospinning solution, core/shell nanofibers were prepared using a custom-made coaxial electrospinning apparatus involving two concentric stainless-steel tubes (Fig. 1). The inner and outer diameters were 0.99 mm and 1.47 mm, respectively for the inner tube while the inner and outer diameters were 2.42 mm and 2.78 mm, respectively for the outer tube. The flow rate was set at 0.015 mL/min and 0.030 mL/min for core and shell part, respectively. A grounded, rotating stainless-steel plate covered with aluminum foil was placed about 25 cm away from the spinneret to collect nanofibers in the form of a mat. A stable Taylor cone was obtained with an applied voltage of 19.5 kV. For systematic investigation and comparison purposes, three different mat configurations were prepared. In configuration A, 7 h of electrospinning with the coaxial setup and the core/shell solutions was used to make a mat involving vancomycin/flurbiprofen core/shell nanofibers. In configuration B, 2 h of electrospinning was first carried out using the shell part of the electrospinning solution, followed by 3 h of electrospinning with the coaxial setup and the core/shell solutions, and finally followed by 2 h of electrospinning with the shell part again to form a mat with a symmetric sandwich geometry. Configuration C was same as the configuration B except that in the middle section, 3 h of electrospinning with just the core part of the solution was used, rather than electrospinning with the coaxial setup and core and shell solutions. Before any further experiments, samples were treated with the mixture of methanol:water vapor (80/20, v/v) to induce the formation of β-sheets in the silk fraction of nanofibers. The evaporation was induced by locally superheating the mixture of methanol/water to 300 °C for 2 h

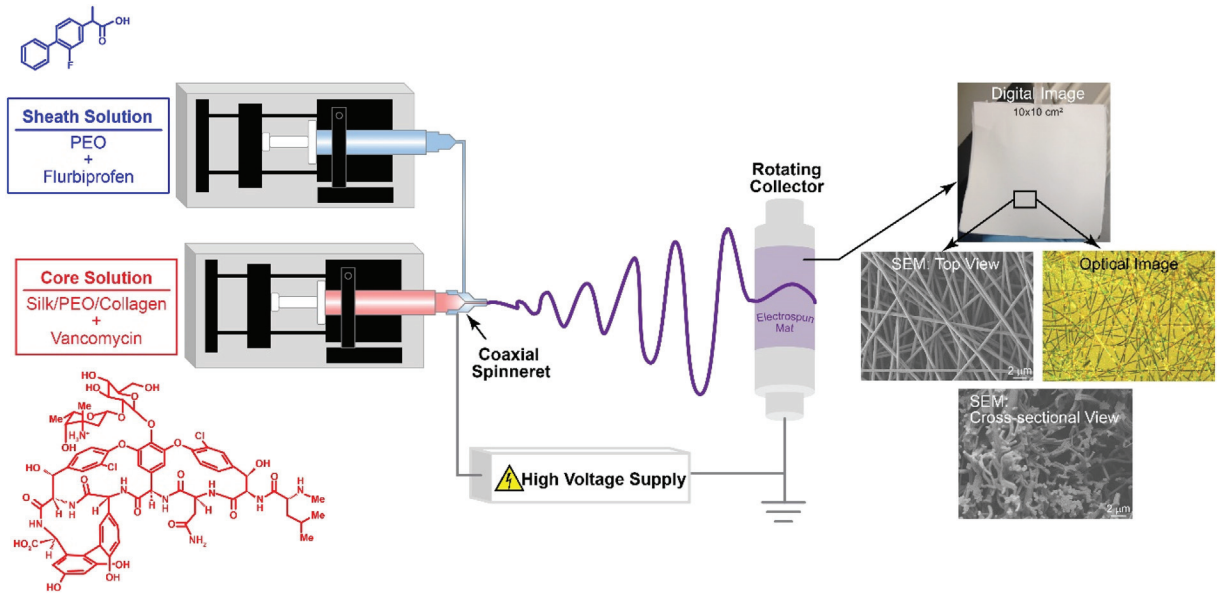

Fig. 1. Schematic illustration of the custom-made coaxial electrospinning apparatus. The chemical structures of anti-inflammatory agent, flurbiprofen (dispersed in sheath solution shown in blue) and anti-bacterial agent, vancomycin (dispersed in core solution shown in red) are displayed right next to solution reservoirs. The digital image, scanning electron micrographs (top as well as cross-sectional views), and optical image of core-shell electrospun mat are shown in the right side of the figure. Enlarged image of cross-sectional view is given in Fig. 3. (For interpretation of the references to color in this figure legend, the reader is referred to the web version of this article.)

and exposing the mats to the vapor.

2.5. In vitro incubation assay and quantification of drug release

After post-treatment, mats were cut into 1 cm × 1 cm pieces, placed in a dialysis membrane (Slide-A-Lyzer™ MINI Dialysis Device Kit, Thermo fisher scientific, MA), and incubated in a 1.5 mL volume of centrifuge tube against 1.2 mL phosphate buffered saline (PBS) solution (pH 7.4) at 37 °C. PBS solution was replaced with a fresh solution at predetermined time points. The PBS solution with released drugs was analyzed by high performance liquid chromatography (HPLC, Agilent Technologies HPLC, 1100 series) using a C18 reverse phase column (Supelco, Milford, MA) coupled with UV/vis detection to quantify the concentrations of vancomycin and flurbiprofen separately. Each sample was run for 10 min with the mobile phase of acetonitrile and PBS (30/70, v/v) with a flow rate of 1 mL/min. The absorbance was monitored at 248 nm for flurbiprofen and 220 nm for vancomycin respectively. The final concentrations were determined using the calibration curves generated with standards of known vancomycin and flurbiprofen concentrations. All samples were assayed in triplicates.

2.6. Structural, chemical, thermal, and mechanical characterization of the core-shell electrospun mats

Attenuated Total Reflectance - Fourier Transform Infrared Spectroscopy (ATR-FTIR) measurements were performed using a Nicolet 6700 Fourier Transform Infrared Spectrometer (Thermo Fisher Scientific Inc., Rockford, IL) with a Deuterated Triglycine Sulfate (DTGS) detector and a grazing angle ATR accessory (VariGATR™, Harrick Scientific Products, Inc., NY) to identify changes in secondary structure of silk protein polymers before and after methanol vapor treatment. The quantitative analysis on respective secondary structures was carried out using the Fourier Self Deconvolution (FSD) fitting method [50] in OMNIC software. This analysis was carried out using Origin 9.0 software (OriginLab Corporation, Northampton, USA). The peak areas were calculated using Peak Analyzer Plug-in (OriginLab) with a straight-line base correction option.

The morphology of nanofibers and core-shell electrospun mats were investigated using scanning electron microscopy (SEM, JEOL-7401, Japan). The samples were coated with 10 nm Au layer to introduce electrical conducting layer prior to SEM. The diameters of core and shell part of electrospun fibers were evaluated by Image J software (NIH). The core-shell structure of electrospun fiber was further characterized using transmission electron microscope (TEM, JSM-1230, Japan) with an accelerating voltage of 120 KV. Samples for the TEM analysis were prepared by directly spun onto a carbon film coated copper grid (Ted Pella, Inc.) for several seconds. After that, the copper grid was left dry overnight in vacuum prior to taking TEM images. The phase behaviors and morphological changes of core-shell electrospun mats as a function of incubation time as well as upon methanol vapor treatment were probed using differential scanning calorimetry (DSC, Q2000, TA instrument, New Castle, DE).

Mechanical properties of samples were tested using a universal tester (5567, Instron, Norwood, MA). Electrospun mats were cut into rectangular strips (40 mm × 7 mm × 0.1 mm) and stored in vacuum prior to tensile test to prevent absorption of water from ambient atmosphere. The rectangular strips were then mounted on a custom-made hollow cardboard holder of which side edges were cut prior to the stress-strain analysis. All tensile tests were performed with strain rate of 1 mm/min at ambient temperature and within 10 min after the electrospun mat was removed from vacuum. The measurements were carried out using a 500-Newton (N) load cell. All measurements were repeated with three samples (strips) for each condition. The generated data was analyzed with Bluehill software v2.

3. Results and discussion

3.1. Structural characterization of mats involving core-shell architecture

The coaxial electrospinning of PEG and silk solutions resulted in nanofibers with a relatively narrow size distribution having the mean fiber diameter of 422 nm and the standard deviation of 74 nm (Fig. 2(a)). The exposure of PEG/silk core-shell nanofibers to methanol vapor caused the axial curvature to significantly increase as evidenced by the transformation from a mostly straight network to a curly and wavy one (Fig. 2(b)). In addition, the average fiber diameter decreased

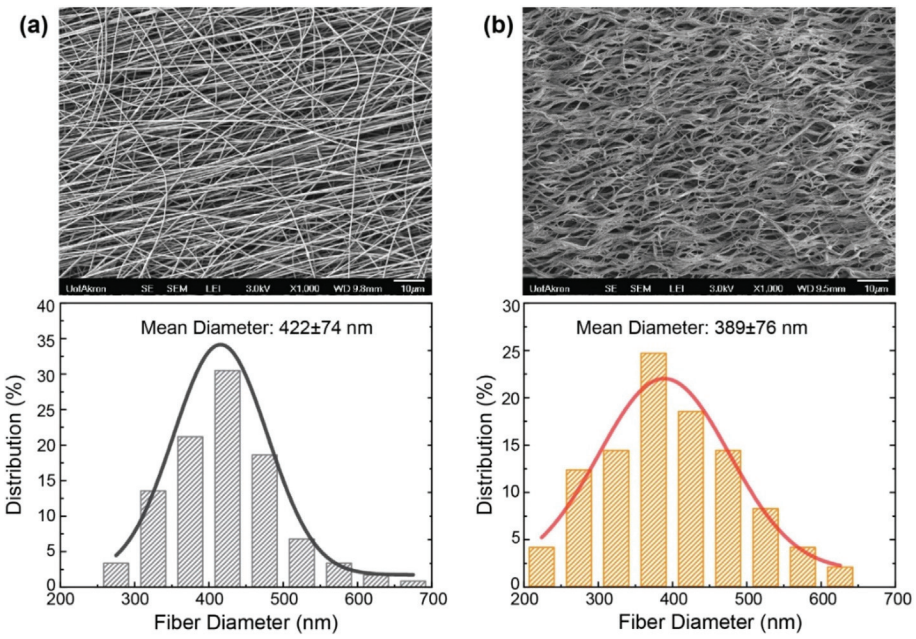

Fig. 2. SEM images and diameter distribution (mean diameter ± standard deviation) of core-shell electrospun mat **(a)** before and **(b)** after methanol vapor treatment for 1 h. The diameters of the nanofibers were measured using Image J [National Institute of Health (NIH)] software and plotted the results as histograms showing the relative fraction of fibers within a certain diameter range. The solid curves are the fitted lines according to the Gaussian distribution with the fitted parameters of mean fiber diameters as listed in the inset.

from 422 ± 74 nm to 389 ± 76 upon methanol vapor treatment. The mechanistic reasons behind these morphological transformations will be discussed later on.

The formation of core/shell structure was confirmed via the cross-sectional fractional SEM and TEM images (Fig. 3). The subsequent image analysis on SEM micrographs revealed that the thickness values of the core and shell layers of the methanol vapor treated nanofibers were 272 ± 44 nm and 107 ± 30 nm, respectively (Fig. 3(a)). Noticeable variations in relative thickness of each layer and non-uniform distribution of thickness along the radial direction within a cross-section were also observed, presumably owing to the capillary waves induced by Taylor instability. TEM image further confirmed the core-shell structure of electrospun nanofibers in a nondestructive manner. The core diameter of the nanofiber was estimated around 250 nm with the approximate sheath thickness of 75 nm, leading to the total dimeter of around 400 nm (Fig. 3 (b)), which are in good agreements with the values estimated from SEM images.

3.2. Release kinetics of active ingredients from electrospun core-shell fiber mats

The effective treatment of wounds requires a well-planned administration of anti-inflammatory and anti-bacterial agents. To evaluate the modulability of core-shell electrospun mats in the aspect of release kinetics, three different mat configurations have been explored (See Fig. 4): 100% of the mat is made from vancomycin/flurbiprofen core/shell nanofibers (Configuration A), the inner mat, which accounts for 60% of the total volume, is made from vancomycin/flurbiprofen core/shell nanofibers while the outer mat, which is 40% of the total volume, is made from sole flurbiprofen nanofibers (Configuration B), and the inner mat (60% of the total volume), is made from sole vancomycin nanofibers while the outer mat (40% of the total volume) is made from sole flurbiprofen nanofibers (Configuration C). For all these three configurations, the release profiles followed a general empirical Weibull equation which describes drug dissolution and release processes from any solid pharmaceutical dosage forms [51]:

$$C(t) = C_o\left[1 - \exp\left(-\frac{(t - t_{lag})^n}{\tau}\right)\right], \quad (1)$$

where C_o indicates the total amount of drug being released from the mat, $C(t)$ is the amount of drug released at time t, and τ is the characteristic decay time (i.e., the inverse of the release rate constant or time constant, defining the time scale of the release process). The t_{lag} accounts for the lag time before the onset of the dissolution or release process which was not observed in any of our electrospun mat configurations and therefore, was considered as being zero in our study. The parameter of n describes the shape of the release curves, all of which follow an exponential trend ($n = 1$) with the R-squared value of 0.99. For the Configuration A (Fig. 4a), the release of flurbiprofen was much faster than that of vancomycin with a time constant of 1.8 ± 0.1 days

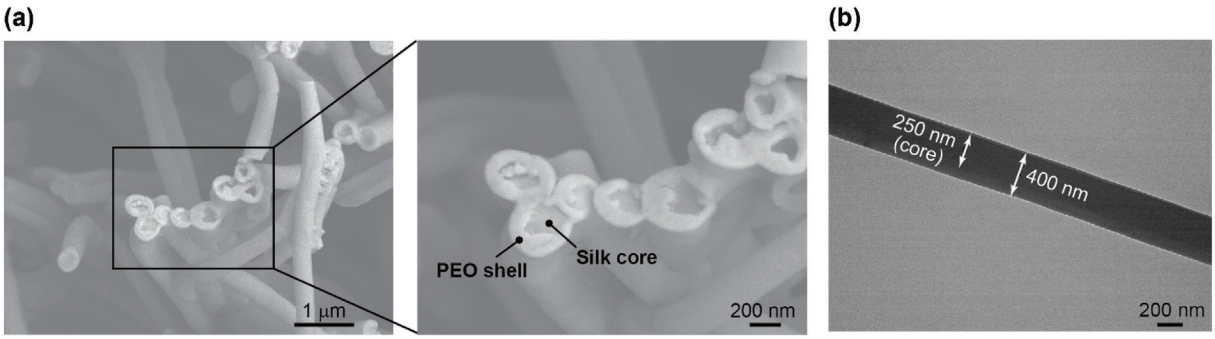

Fig. 3. Representative **(a)** high-resolution SEM and **(b)** TEM images indicating core and shell layers of electrospun nanofibers. The core compartment contains a mixture of three components of silk: collagen: PEO = 89:5:6 (weight ratio) while the shell region consists of pure PEO as a macromolecular structural building unit.

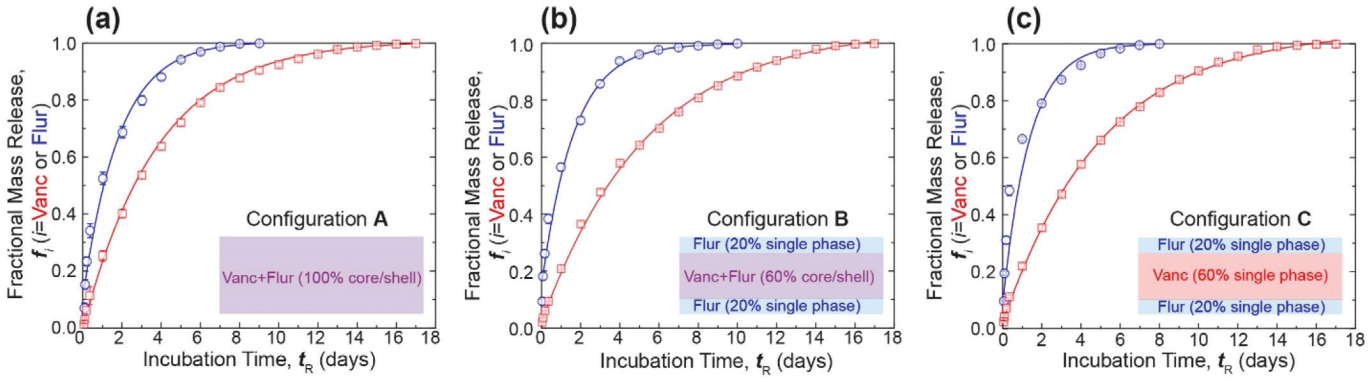

Fig. 4. Fractional release of vancomycin (Vanc: □) and flurbiprofen (Flur: ○) in three different mat configurations: **(a)** 100% of the mat is made from vancomycin/flurbiprofen core/shell nanofibers (Configuration A), **(b)** the inner mat, which accounts for 60% of the total volume, is made from vancomycin/flurbiprofen core/shell nanofibers while the outer mat, which is 40% of the total volume, is made from flurbiprofen nanofibers (Configuration B), and **(c)** the inner mat (60% of the total volume), is made from vancomycin nanofibers while the outer mat (40% of the total volume) is made from flurbiprofen nanofibers (Configuration C). The cumulated amount of vancomycin or flurbiprofen released from three different types of electrospun mats was first normalized by the area (size) of mats and later converted to the fractional release (f_{Vanc} or f_{Flur}), which represents the fraction of released amount of vancomycin or flurbiprofen at a certain time point (t_R) to the final release quantity. For a fixed total processing time (7 h), different configurations resulted in different active ingredient concentrations since the volumes of compartments where respective drugs were incorporated were different. Percent release data can be converted to the actual concentrations considering that 100% vancomycin and flurbiprofen release corresponds to 72.2 μg/cm^2 and 13.8 μg/cm^2 in Configuration A, 33.1 μg/cm^2 and 13.4 μg/cm^2 in Configuration B, and 33.4 μg/cm^2 and 9.0 μg/cm^2 in Configuration C, respectively.

compared to 3.8 ± 0.1 days. For the Configuration B (Fig. 4b), the release of flurbiprofen had a release time-constant of 1.7 ± 0.1 days, which is comparable with Configuration A. On the other hand, the release of vancomycin slowed down with a time constant of 5.4 ± 0.1 days. Finally, in the case of Configuration C (Fig. 4c), the time constants of release were 1.4 ± 0.1 and 5.1 ± 0.1 days for flurbiprofen and vancomycin, respectively.

The abovementioned trends can be explained by considering diffusion of molecules in macromolecular matrices, disintegration/dissolution of PEO shell layer, and swelling of silk core compartment. For all configurations, the inter-fiber spacing spans the range of 0.1 to 1 μm within an electrospun mat (See Fig. 2), which is several orders of magnitude larger than the size of drug molecules. Therefore, the transport of drug molecules from outermost surface of fibers to outermost surface of the mat should follow a diffusional behavior in bulk once the mat is saturated with water. Hence, the radial transport of the drug molecules within the nanofibers is to be a rate determining step which should be responsible for the observed release profiles. For all configurations, molecular diffusion through polymeric matrices (silk or PEO) will contribute to the mass transport phenomena to a certain extent with some variations depending on the type of matrix and configuration of mat. The rate of molecular diffusion within polymeric materials depends upon the size and shape of the diffusing molecules as well as internal nanostructures and pore/mesh length scales of the matrix material [52,53]. The fact that the molecular weight of flurbiprofen and vancomycin is 244 Da and 1449 Da, respectively [54] can partly account for the larger release rates of flurbiprofen. However, the primary reason of displaying a faster release from PEO shell layer is likely due to the hydrophilic nature of PEO by its dissolution once in contact with water (or physiological fluid) [55,56]. On the other hand, silk fibroin (the major constituent in the core layer) is water-insoluble protein with biodegradable properties which can be controlled by the interplay among β-sheet content, hydrophilic interaction with water molecules, and hierarchical crystal-noncrystal alternating nanostructures [57]. For silk fibroins with a large β-sheet content, onset of degradation initiates in a timeframe of weeks to months in vivo [58]. Hence, the diffusion process is expected to be the dominant transport mechanism for vancomycin through nanofiber cores. However, considering silk fibroin partially swells in the presence of water [59], the resultant variations in the characteristic mesh size suggest a time-dependent diffusion coefficient for the case of vancomycin.

Now, the relative differences in release time constant of flurbiprofen and vancomycin with respect to mat configuration can be elucidated via nanostructural and geometrical arguments. For the Configuration A, there is a single type of fibers involved in the wound dressing mat: core/shell nanofibers with a core containing collagen, silk, PEO, and vancomycin and a shell consisting of PEO and flurbiprofen. For the case of configuration B, the mat is anisotropic in the normal direction, i.e., the outer layer containing flurbiprofen nanofibers is directly in contact with water while the inner layer containing vancomycin/flurbiprofen core/shell nanofibers is initially surrounded by interstitial air trapped between fibers upon contacting with water. The time needed for water molecules to penetrate and displace hydrophobic air pockets in the proximity of the network of nanofibers can be the one of the reasons behind slowing down of vancomycin release. For the Configuration C, the release rate of both vancomycin is slightly faster compared to the Configuration B. The absence of PEO shell can not only remove the additional diffusion barrier for water but also reduce the radial stress and Laplace pressure applied on silk-rich core. Both of these effects can facilitate the swelling of silk and increase the effective mesh size, thereby leading to a faster release of vancomycin.

Our release studies clearly indicate that the release timescales and thus, released amounts of respective wound healing agents at different time points are controllable depending on material choice as well as design and configuration of electrospun mat as intended. Furthermore, we note that those release timescales for all configurations are suitable for reducing pains associated with the inflammatory response as well for preventing bacterial infections commonly occurring before mid/late proliferation phase of wound healing.

3.3. Mechanical properties of electrospun core-shell fiber mats

As the human body, joints, and muscles are in constant motion, dressings/mats/nets used for protecting and treating wounds tend to experience a lot of deformation, stretching, and mechanical stress. As such, the mechanical reliability, robustness, and flexibility for user comfort are another critical aspect to consider for designing advanced wound healing dressings. In this context, we have studied the stress-strain behavior of the mats involving core/shell nanofibers after methanol vapor treatment as a function of water incubation time (Fig. 5). Mats containing vancomycin/flurbiprofen (core/shell nanofibers) had a tensile modulus of 185 MPa, which was increased with incubation time

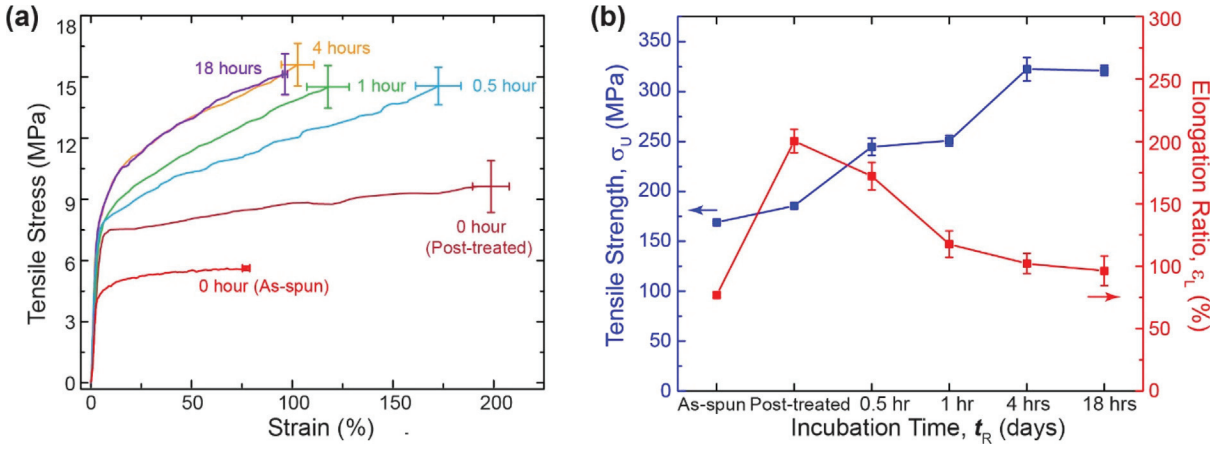

Incubation Time, t_R (hours)	Tensile Modulus (E_M, MPa)	Tensile Strength (σ_U, MPa)	Elongation Ratio (ε_L, %)
0 (As-is)	169.4 ± 1.0	5.6 ± 0.1	77.1 ± 1.9
0 (No incubation)	185.3 ± 2.0	11.3 ± 0.4	200.8 ± 9.1
0.5	245.1 ± 8.5	14.6 ± 0.9	172.5 ± 11.2
1	250.8 ± 5.4	14.5 ± 1.0	117.7 ± 10.5
4	323.5 ± 11.9	15.6 ± 1.0	102.7 ± 8.1
18	322.8 ± 4.9	15.1 ± 1.0	96.43 ± 11.8
Human Skin	15-150	5-30	35-115

Fig. 5. (a) Stress-strain curves of the mats involving core/shell nanofibers as a function of incubation time under physiological experimental conditions and **(b)** changes in tensile strength (σ_U) and elongation ratio (ε_L) as a function of incubation time, t_R. Summary data of mechanical properties of core-shell electrospun mats are shown in the table and compared with those of human skin [60].

and eventually reaching a plateau after 4 h of incubation. This trend can be ascribed to the leaching of PEO from nanocomposite fibers during a course of incubation, leaving out mechanically more robust components in the system, i.e. silk and collagen.

Tensile strength of the mats was measured as 11.3 MPa after methanol vapor treatment (Post-treated), which was enhanced by about 104% from the one before methanol vapor treatment (As-spun or As-is) and also increased but showing less variations with incubation time (Fig. 5b). While the mats initially demonstrated a percent elongation-to-break of about 201%, increasing incubation time resulted in a reduction of the percent elongation-to-break, eventually reaching down to approximately 96% after 18 h of incubation (Fig. 5b). It is noteworthy that the core-shell electrospun mats were more compliant and flexible than human skin and had similar elongational properties, indicating their desirable mechanical characteristics over a period of incubation carried out under physiological experimental conditions (PBS pH 7.4 and 37 °C).

While prior studies have observed that the modulus values of polymeric materials and polymer composites are generally reduced when in contact with moisture and water [61–64], it is intriguing to observe that the modulus of core-shell electrospun mat has been enhanced with increasing the incubation time (exposure time to surrounding media of PBS, i.e. water). As incubation goes on, the most soluble component, i.e. PEO will be readily leached out from the composite nanofibers which are made of PEO, silk, and collagen, making the composite nanofibers relatively richer in silk and collagen. To support this scenario, we assessed the phase behavior and enthalpy of melting of the mats as a function of incubation time by DSC (Fig. 6a) of which sample mats were obtained from identical experimental setups as for mechanical test studies. The DSC peak located around 64 °C for core/shell nanofiber mat before incubation indicates the melting of PEO, of which magnitude decreases as a function of incubation time in an exponential fashion (Fig. 6b). Such a depression in melting points of PEO is most likely to be due to the Gibbs-Thomson effect [65] where nanoscale roughness forms on nanofibers via the dissolution of PEO component in a stochastic fashion and introduces new curvature distribution larger than the curvature of nanofibers (i.e. 1/radius). Given that the time-evolved dissolution of PEO leads that the relative amounts of silk and collagen would increase in the nanocomposite structure and silk and collagen have the higher modulus values than the one of PEO [64,66,67], increases in modulus values observed from stress-strain curves (Fig. 5) can be interpreted in light of the effective medium theory of composites [68–70].

3.4. Mechanistic studies on the effect of methanol vapor treatment on core/shell nanofiber mats

As seen from mechanical test data (Fig. 5) along with release profiles (Fig. 4), methanol vapor treatment of core/shell nanofibers turns out to be essential to achieve long-term and reliable release profiles. In order to relate improved release properties to mechanistic insights of core/shell electrospun mats, we carried out a complementary spectroscopic analysis by FTIR. The FTIR spectroscopy and subsequent detailed analysis of secondary structure in silk were performed to determine any changes in the vibrational modes of the macromolecules upon their exposure to methanol vapor (Figs. 7a and b) and then as a function of incubation time (Fig. 7c). The C═O (70–85%) and C−N (10–20%) groups gave rise to strong, multiple peaks in the region of 1600–1700 cm^{-1}, which is referred as amide I band stemming from α-helix, β-sheet, random, side, and turns structures of proteins. Considering that the amount of silk protein is about twenty times larger than that of collagen, these peaks are primarily attributed to silk protein. The deconvolution of sub-components amide I band revealed that the contribution of β-sheets increased from 22% to 32% while the

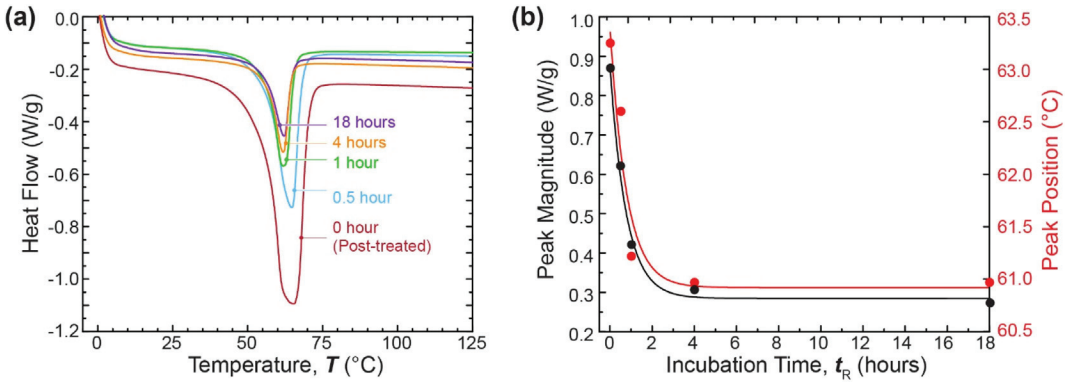

Fig. 6. (a) DSC thermograms of core/shell nanofiber mats with respect to incubation time. **(b)** Corresponding peak magnitude and position data (black and red circles, respectively) obtained by a Gaussian peak fitting algorithm from Fig. (a). Black and red solid lines represent the fittings of the magnitude and position data with an exponential decay function. Both magnitude and position of the DSC peak decreases exponentially as a function of incubation time (t_R) with an exponential decay constant, τ of 0.78 and 0.77 h, respectively. (For interpretation of the references to color in this figure legend, the reader is referred to the web version of this article.)

contribution of α-helix and random structures decreased from 24% to 23% and from 25% to 17%, respectively upon methanol vapor treatment (Post-treated). In other words, a significant fraction of random and α-helix protein structures was converted into *β*-sheet structures. There was minor decrease in the fraction of turns structure and minor increase the fraction of side structure. Molecular diffusion generally slows down transitioning from a more amorphous matrix to a more crystalline matrix [53,71,72]. As a higher fraction of *β*-sheet structures indicated a higher crystallinity in proteins [73–76], the prolonged release profiles of active ingredients upon methanol vapor treatment can be explained by crystallization-induced retardation of the molecular diffusion. Furthermore, a significant increase in *β*-sheet contents was observed whereas the signals for other secondary structures (especially, random and *α*-helix) in silk proteins were rather decreased as a function of incubation time (Fig. 7c). This data indicates that the transformation from amorphous to crystalline internal structures also caused by an annealing mechanism of water molecules could further slow down the release of therapeutic incorporated in the core (i.e. vancomycin) as observed in Fig. 4.

As a complementary technique, the DSC was used to study the influence of methanol vapor treatment on the nanostructural changes of core/shell electrospun mats (Fig. 8). The thermograms exhibited two distinct peaks at ~64 °C and ~282 °C in the first scan for both before (As-is) and after methanol vapor treatment (Post-treated). The subsequent (secondary) DSC scans (not shown here) resulted in only single peak around 64 °C, indicating that the second peak has been associated with an irreversible process, presumably pertaining to the decomposition of components. Considering the literature data on thermal analysis of PEO and silk [77–80], the former (~64 °C) is assigned to the melting of PEO while the latter (~282 °C) is the decomposition and degradation of silk fibroin with random coil conformation (degradation peaks associated with well oriented *β*-sheets occur at and above 300 °C [81] which were not experimentally accessible). While the treatment caused the onset of decomposition temperature for silk fibroins shifted from 260 °C to 269 °C and also the heat of decomposition decreased from 45.2 J/g to 29.4 J/g, no significant changes were observed on the onset of melting and the heat of melting for PEO components. The relative amounts of the silk I conformations and silk II crystals (*β*- sheets) are reported to determine the stability with respect to the changes in temperature i.e. the higher *β*-sheet content is known to increase the decomposition temperature of silk fibroin [80,82,83]. Indeed, our observations on DSC thermograms show good agreements with previous findings, i.e., exposure to methanol induced structural transitions from silk I to silk II, giving rise to the higher *β*-sheet content and crystallinity as observed. Overall, the combination of FTIR and DSC studies confirmed that the methanol vapor treatment leads to critical structural transitions in silk fibroin building blocks in core/shell nanofibers, thereby allowing a slower and gradual release of active ingredients through a crystalline matrix.

4. Conclusions

In this work, we demonstrate the proof-of-concept where vancomycin and flurbiprofen can be loaded in the core and shell sections of

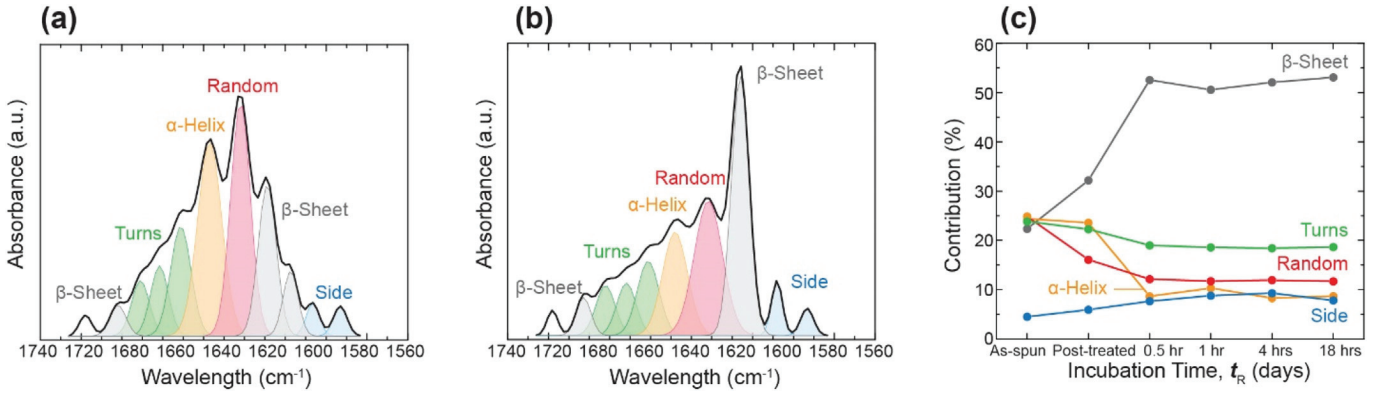

Fig. 7. Representative results of a Fourier self–deconvolution analysis on the Amide *I* region for core/shell electrospun mats **(a)** before (As-is) and **(b)** after methanol vapor treatment (Post-treated). The assignments of the various peaks to the different elements of secondary structure are shown with color-coordinated texts (labels). **(c)** Percentage change of different secondary structures in core/shell nanofibers as a function of incubation time, t_R.

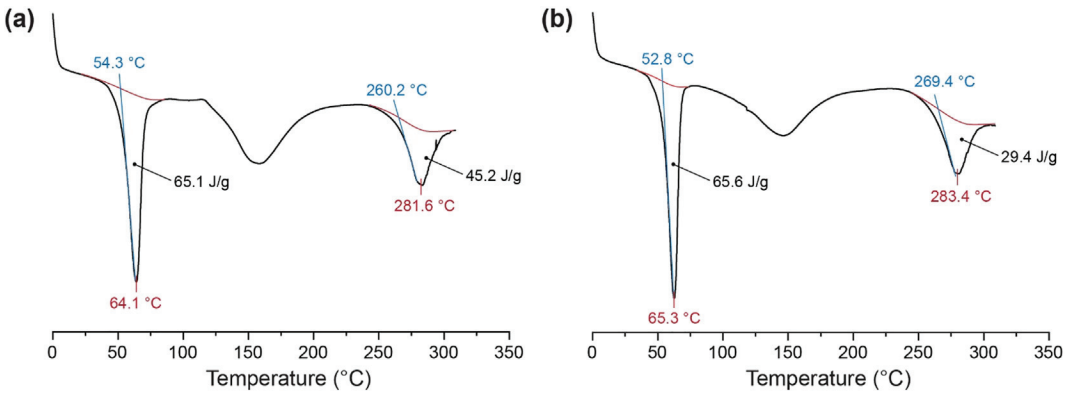

Fig. 8. DSC thermograms of core/shell electrospun mats **(a)** before (As-is) and **(b)** after treatment of methanol vapor (Post-treated).

nanofibers prepared by co-axial electrospinning process. The faster release kinetics needed for anti-inflammatory agent, flurbiprofen was achieved by selectively placing it on the shell layer of a hydrophilic polymer, polyethylene oxide. The slower release of vancomycin was accomplished by localizing this therapeutic agent in the core of nanofibers and relying on crystalline silk fibroin matrix, which delays the diffusion of molecules. The release profiles of the core/shell electrospun mats developed in three different configurations all followed an exponential trend, which is indicative of a first-order process with a Fickian diffusional characteristics. The ratio of time constants of vancomycin to the ones of flurbiprofen was able to be controlled from about 2 to 4 depending on the configurations (architectures) of core/shell electrospun mats, i.e. 1.8 ± 0.1 days (~9 days for 99% release) for flurbiprofen in comparison to a time constant 3.8 ± 0.1 days (~17 days for 99% release) for vancomycin. Mats containing vancomycin/flurbiprofen core/shell nanofibers showed much improved tensile modulus and strength after methanol vapor treatment, both of which were further increased with incubation time whereas the initial elongation ratio of about 201% displayed a temporal reduction, eventually reflecting comparable features in flexibility with human skin. Such desirable release kinetics and mechanical properties were attributable to several factors; transition of secondary structures from silk I conformations to β-sheets by exposure to methanol vapor as well as water annealing with time, selective compartmentalization of each therapeutic agent into distinct matrix pairs chosen with cares, and core/shell electrospun mats with characteristic architectures. Overall, the core/shell electrospun mats newly developed here hold a dual-functionality, carrying both anti-inflammatory and anti-bacterial agents and address specific medical needs in the field of wound healing, precisely controlling release kinetics of therapeutics incorporated at different time scales from rapid to more prolonged delivery. The design concepts utilized in this study can be applicable to other clinically relevant systems which require multi-drug releasing, ranging from daily medical procedures to battlefield trauma.

Acknowledgements

This project was partially supported by the National Science Foundation (NSF) under Grant Nos. 1511626 and 1826250. Support was also provided by the Donors of the American Chemical Society Petroleum Research Fund.

References

[1] S. Dhivya, V.V. Padma, E. Santhini, Wound dressings–a review, BioMedicine. 5 (2015).
[2] M.C. Robson, D.L. Steed, M.G. Franz, Wound healing: biologic features and approaches to maximize healing trajectories, Curr. Probl. Surg. 38 (2001) 72–140.
[3] G.S. Lazarus, D.M. Cooper, D.R. Knighton, D.J. Margolis, R.E. Pecoraro, G. Rodeheaver, M.C. Robson, Definitions and guidelines for assessment of wounds and evaluation of healing, Arch. Dermatol. 130 (1994) 489–493.
[4] A.J. Singer, A.B. Dagum, Current management of acute cutaneous wounds, N. Engl. J. Med. 359 (2008) 1037–1046.
[5] S. Grim Hostetler, H. Xiang, S. Gupta, C.K. Sen, G.M. Gordillo, Discharge patterns of injury-related hospitalizations with an acute wound in the United States, Wounds 18 (2006) 340–351.
[6] N.S. Greaves, K.J. Ashcroft, M. Baguneid, A. Bayat, Current understanding of molecular and cellular mechanisms in fibroplasia and angiogenesis during acute wound healing, J. Dermatol. Sci. 72 (2013) 206–217.
[7] J. Li, J. Chen, R. Kirsner, Pathophysiology of acute wound healing, Clin. Dermatol. 25 (2007) 9–18.
[8] J.D. Stroncek, W.M. Reichert, Overview of wound healing in different tissue types, Indwelling Neural Implant. Strateg. Contend. with Vivo Environ. (2007) 3–40.
[9] T. Velnar, T. Bailey, V. Smrkolj, The wound healing process: an overview of the cellular and molecular mechanisms, J. Int. Med. Res. 37 (2009) 1528–1542.
[10] G. 2nd Broughton, J.E. Janis, C.E. Attinger, Wound healing: an overview, Plast. Reconstr. Surg. 117 (2006).
[11] K.G. Harding, H.L. Morris, G.K. Patel, Science, medicine, and the future: healing chronic wounds, BMJ Br. Med. J. 324 (2002) 160.
[12] K. Järbrink, G. Ni, H. Sönnergren, A. Schmidtchen, C. Pang, R. Bajpai, J. Car, Prevalence and incidence of chronic wounds and related complications: a protocol for a systematic review, Syst. Rev. 5 (2016) 152.
[13] A.F. Falabella, Debridement and wound bed preparation, Dermatol. Ther. 19 (2006) 317–325.
[14] C.E. Attinger, J.E. Janis, J. Steinberg, J. Schwartz, A. Al-Attar, K. Couch, Clinical approach to wounds: debridement and wound bed preparation including the use of dressings and wound-healing adjuvants, Plast. Reconstr. Surg. 117 (2006) 72S–109S.
[15] S.J. Phillips, Physiology of wound healing and surgical wound care, ASAIO J. 46 (2000) S2–S5.
[16] B.S. Atiyeh, J. Ioannovich, C.A. Al-Amm, K.A. El-Musa, Management of acute and chronic open wounds: the importance of moist environment in optimal wound healing, Curr. Pharm. Biotechnol. 3 (2002) 179–195.
[17] T.K. Hunt, H.W. Hopf, Wound healing and wound infection, what surgeons and anesthesiologists can do, Surg. Clin. North Am. 77 (1997) 587–606.
[18] E.C. Newsom, K.L. Connolly, K.S. Nehal, Facilitating healing of granulating wounds: dressings, dermal substitutes, and other methods, Curr. Dermatol. Rep. 4 (2015) 125–133.
[19] M. Rippon, P. Davies, R. White, Taking the trauma out of wound care: the importance of undisturbed healing, J. Wound Care 21 (2012).
[20] A. Sood, M.S. Granick, N.L. Tomaselli, Wound dressings and comparative effectiveness data, Adv. Wound Care. 3 (2014) 511–529.
[21] E.A. Kamoun, E.-R.S. Kenawy, X. Chen, A review on polymeric hydrogel membranes for wound dressing applications: PVA-based hydrogel dressings, J. Adv. Res. 8 (3) (2017) (271–233).
[22] L.I.F. Moura, A.M.A. Dias, E. Carvalho, H.C. de Sousa, Recent advances on the development of wound dressings for diabetic foot ulcer treatment—a review, Acta Biomater. 9 (2013) 7093–7114.
[23] J.S. Boateng, K.H. Matthews, H.N.E. Stevens, G.M. Eccleston, Wound healing dressings and drug delivery systems: a review, J. Pharm. Sci. 97 (2008) 2892–2923.
[24] V. Jones, J.E. Grey, K.G. Harding, ABC of wound healing: wound dressings, BMJ Br. Med. J. 332 (2006) 777.
[25] M. Brown-Etris, C. Milne, H. Orsted, J.L. Gates, D. Netsch, M. Punchello, N. Couture, M. Albert, E. Attrell, J. Freyberg, A prospective, randomized, multisite clinical evaluation of a transparent absorbent acrylic dressing and a hydrocolloid dressing in the management of stage II and shallow stage III pressure ulcers, Adv. Skin Wound Care 21 (2008) 169–174.
[26] E.A. Nelson, R.J. Prescott, D.R. Harper, B. Gibson, D. Brown, C.V. Ruckley, A factorial, randomized trial of pentoxifylline or placebo, four-layer or single-layer compression, and knitted viscose or hydrocolloid dressings for venous ulcers, J. Vasc. Surg. 45 (2007) 134–141.
[27] S. Moritz, C. Wiegand, F. Wesarg, N. Hessler, F.A. Müller, D. Kralisch, U.-C. Hipler, D. Fischer, Active wound dressings based on bacterial nanocellulose as drug delivery system for octenidine, Int. J. Pharm. 471 (2014) 45–55.

[28] G. Sandri, M.C. Bonferoni, F. D'Autilia, S. Rossi, F. Ferrari, P. Grisoli, M. Sorrenti, L. Catenacci, C. Del Fante, C. Perotti, Wound dressings based on silver sulfadiazine solid lipid nanoparticles for tissue repairing, Eur. J. Pharm. Biopharm. 84 (2013) 84–90.
[29] A.M.A. Dias, A. Rey-Rico, R.A. Oliveira, S. Marceneiro, C. Alvarez-Lorenzo, A. Concheiro, R.N.C. Júnior, M.E.M. Braga, H.C. De Sousa, Wound dressings loaded with an anti-inflammatory jucá (Libidibia ferrea) extract using supercritical carbon dioxide technology, J. Supercrit. Fluids 74 (2013) 34–45.
[30] C. Cencetti, D. Bellini, A. Pavesio, D. Senigaglia, C. Passariello, A. Virga, P. Matricardi, Preparation and characterization of antimicrobial wound dressings based on silver, gellan, PVA and borax, Carbohydr. Polym. 90 (2012) 1362–1370.
[31] A. Agarwal, T.B. Nelson, P.R. Kierski, M.J. Schurr, C.J. Murphy, C.J. Czuprynski, J.F. McAnulty, N.L. Abbott, Polymeric multilayers that localize the release of chlorhexidine from biologic wound dressings, Biomaterials. 33 (2012) 6783–6792.
[32] J.S. Gonzalez, L.N. Ludueña, A. Ponce, V.A. Alvarez, Poly (vinyl alcohol)/cellulose nanowhiskers nanocomposite hydrogels for potential wound dressings, Mater. Sci. Eng. C. 34 (2014) 54–61.
[33] Z. Peles, M. Zilberman, Novel soy protein wound dressings with controlled antibiotic release: mechanical and physical properties, Acta Biomater. 8 (2012) 209–217.
[34] Y. Zhou, H. Yang, X. Liu, J. Mao, S. Gu, W. Xu, Electrospinning of carboxyethyl chitosan/poly (vinyl alcohol)/silk fibroin nanoparticles for wound dressings, Int. J. Biol. Macromol. 53 (2013) 88–92.
[35] R. Zhao, X. Li, B. Sun, Y. Zhang, D. Zhang, Z. Tang, X. Chen, C. Wang, Electrospun chitosan/sericin composite nanofibers with antibacterial property as potential wound dressings, Int. J. Biol. Macromol. 68 (2014) 92–97.
[36] C. Li, R. Fu, C. Yu, Z. Li, H. Guan, D. Hu, D. Zhao, L. Lu, Silver nanoparticle/chitosan oligosaccharide/poly (vinyl alcohol) nanofibers as wound dressings: a preclinical study, Int. J. Nanomedicine 8 (2013) 4131.
[37] A. Vasconcelos, A.C. Gomes, A. Cavaco-Paulo, Novel silk fibroin/elastin wound dressings, Acta Biomater. 8 (2012) 3049–3060.
[38] T. Wang, X.-K. Zhu, X.-T. Xue, D.-Y. Wu, Hydrogel sheets of chitosan, honey and gelatin as burn wound dressings, Carbohydr. Polym. 88 (2012) 75–83.
[39] M. Tummalapalli, M. Berthet, B. Verrier, B.L. Deopura, M.S. Alam, B. Gupta, Composite wound dressings of pectin and gelatin with aloe vera and curcumin as bioactive agents, Int. J. Biol. Macromol. 82 (2016) 104–113.
[40] K.A. Rieger, N.P. Birch, J.D. Schiffman, Designing electrospun nanofiber mats to promote wound healing–a review, J. Mater. Chem. B 1 (2013) 4531–4541.
[41] A.R. Unnithan, G. Gnanasekaran, Y. Sathishkumar, Y.S. Lee, C.S. Kim, Electrospun antibacterial polyurethane–cellulose acetate–zein composite mats for wound dressing, Carbohydr. Polym. 102 (2014) 884–892.
[42] F. Zheng, S. Wang, S. Wen, M. Shen, M. Zhu, X. Shi, Characterization and antibacterial activity of amoxicillin-loaded electrospun nano-hydroxyapatite/poly (lactic-co-glycolic acid) composite nanofibers, Biomaterials. 34 (2013) 1402–1412.
[43] A. Celebioglu, O.C.O. Umu, T. Tekinay, T. Uyar, Antibacterial electrospun nanofibers from triclosan/cyclodextrin inclusion complexes, Colloids Surf. B: Biointerfaces 116 (2014) 612–619.
[44] M. Montazer, S.B. Malekzadeh, Electrospun antibacterial nylon nanofibers through in situ synthesis of nanosilver: preparation and characteristics, J. Polym. Res. 19 (2012) 9980.
[45] A. Schneider, X.Y. Wang, D.L. Kaplan, J.A. Garlick, C. Egles, Biofunctionalized electrospun silk mats as a topical bioactive dressing for accelerated wound healing, Acta Biomater. 5 (2009) 2570–2578.
[46] E.S. Troullos, K.M. Hargreaves, D.P. Butler, R.A. Dionne, Comparison of nonsteroidal anti-inflammatory drugs, ibuprofen and flurbiprofen, with methylprednisolone and placebo for acute pain, swelling, and trismus, J. Oral Maxillofac. Surg. 48 (1990) 945–952.
[47] K.-M. Park, M.-K. Lee, K.-J. Hwang, C.-K. Kim, Phospholipid-based microemulsions of flurbiprofen by the spontaneous emulsification process, Int. J. Pharm. 183 (1999) 145–154.
[48] M.L. Campbell, D. Marchaim, J.M. Pogue, B. Sunkara, S. Bheemreddy, P. Bathina, H. Pulluru, N. Chugh, M.N. Wilson, J. Moshos, Treatment of methicillin-resistant Staphylococcus aureus infections with a minimal inhibitory concentration of 2 μg/mL to vancomycin: old (trimethoprim/sulfamethoxazole) versus new (daptomycin or linezolid) agents, Ann. Pharmacother. 46 (2012) 1587–1597.
[49] D.N. Rockwood, R.C. Preda, T. Yücel, X. Wang, M.L. Lovett, D.L. Kaplan, Materials fabrication from Bombyx mori silk fibroin, Nat. Protoc. 6 (2011) 1612–1631.
[50] X. Hu, D. Kaplan, P. Cebe, Determining beta-sheet crystallinity in fibrous proteins by thermal analysis and infrared spectroscopy, Macromolecules. 39 (2006) 6161–6170.
[51] P. Costa, J.M. Sousa Lobo, Modeling and comparison of dissolution profiles, Eur. J. Pharm. Sci. 13 (2001) 123–133.
[52] N. Lorén, M. Nydén, A.M. Hermansson, Determination of local diffusion properties in heterogeneous biomaterials, Adv. Colloid Interf. Sci. 150 (2009) 5–15.
[53] E. Oral, K.K. Wannomae, S.L. Rowell, O.K. Muratoglu, Diffusion of vitamin E in ultra-high molecular weight polyethylene, Biomaterials. 28 (2007) 5225–5237.
[54] J.H. Kang, D.H. Oh, Y.-K. Oh, C.S. Yong, H.-G. Choi, Effects of solid carriers on the crystalline properties, dissolution and bioavailability of flurbiprofen in solid self-nanoemulsifying drug delivery system (solid SNEDDS), Eur. J. Pharm. Biopharm. 80 (2012) 289–297.
[55] A.V. Kabanov, S.V. Vinogradov, Y.G. Suzdaltseva, V.Y. Alakhov, Water-soluble block polycations as carriers for oligonucleotide delivery, Bioconjug. Chem. 6 (1995) 639–643.
[56] Z. Li, X.J. Loh, Water soluble polyhydroxyalkanoates: future materials for therapeutic applications, Chem. Soc. Rev. 44 (2015) 2865–2879.
[57] Q. Lu, B. Zhang, M. Li, B. Zuo, D.L. Kaplan, Y. Huang, H. Zhu, Degradation mechanism and control of silk fibroin, Biomacromolecules. 12 (2011) 1080–1086.
[58] G.S. Perrone, G.G. Leisk, T.J. Lo, J.E. Moreau, D.S. Haas, B.J. Papenburg, E.B. Golden, B.P. Partlow, S.E. Fox, A.M.S. Ibrahim, The use of silk-based devices for fracture fixation, Nat. Commun. 5 (2014).
[59] K. Kosmidis, P. Argyrakis, P. Macheras, A reappraisal of drug release laws using Monte Carlo simulations: the prevalence of the Weibull function, Pharm. Res. 20 (2003) 988–995.
[60] J. Pan, N. Liu, H. Sun, F. Xu, Preparation and characterization of electrospun PLCL/poloxamer nanofibers and dextran/gelatin hydrogels for skin tissue engineering, PLoS One 9 (2014) e112885.
[61] K. Hosaka, J. Tagami, Y. Nishitani, M. Yoshiyama, M. Carrilho, F.R. Tay, K.A. Agee, D.H. Pashley, Effect of wet vs. dry testing on the mechanical properties of hydrophilic self-etching primer polymers, Eur. J. Oral Sci. 115 (2007) 239–245.
[62] G. Baschek, G. Hartwig, F. Zahradnik, Effect of water absorption in polymers at low and high temperatures, Polymer (Guildf). 40 (1999) 3433–3441.
[63] A.J. Nolte, N.D. Treat, R.E. Cohen, M.F. Rubner, Effect of relative humidity on the Young's modulus of polyelectrolyte multilayer films and related nonionic polymers, Macromolecules. 41 (2008) 5793–5798.
[64] T.F. Otero, J.J.L. Cascales, G.V. Arenas, Mechanical characterization of free-standing polypyrrole film, Mater. Sci. Eng. C. 27 (2007) 18–22.
[65] F. Han, S. Li, R. Yin, H. Liu, L. Xu, Effect of surfactants on the formation and characterization of a new type of colloidal drug delivery system: nanostructured lipid carriers, Colloids Surf. A Physicochem. Eng. Asp. 315 (2008) 210–216.
[66] L.S. Wray, J. Rnjak-Kovacina, B.B. Mandal, D.F. Schmidt, E.S. Gil, D.L. Kaplan, A silk-based scaffold platform with tunable architecture for engineering critically-sized tissue constructs, Biomaterials. 33 (2012) 9214–9224.
[67] X. Chen, Y.-Y. Qi, L.-L. Wang, Z. Yin, G.-L. Yin, X.-H. Zou, H.-W. Ouyang, Ligament regeneration using a knitted silk scaffold combined with collagen matrix, Biomaterials. 29 (2008) 3683–3692.
[68] H.L. Duan, X. Yi, Z.P. Huang, J. Wang, A unified scheme for prediction of effective moduli of multiphase composites with interface effects. Part I: theoretical framework, Mech. Mater. 39 (2007) 81–93.
[69] E.J. Garboczi, J.G. Berryman, Elastic moduli of a material containing composite inclusions: effective medium theory and finite element computations, Mech. Mater. 33 (2001) 455–470.
[70] J.W. Ju, T.M. Chen, Micromechanics and effective moduli of elastic composites containing randomly dispersed ellipsoidal inhomogeneities, Acta Mech. 103 (1994) 103–121.
[71] M. Drieskens, R. Peeters, J. Mullens, D. Franco, P.J. Lemstra, D.G. Hristova-Bogaerds, Structure versus properties relationship of poly (lactic acid). I. Effect of crystallinity on barrier properties, J. Polym. Sci. B Polym. Phys. 47 (2009) 2247–2258.
[72] R. Kumar, H. Münstedt, Polyamide/silver antimicrobials: effect of crystallinity on the silver ion release, Polym. Int. 54 (2005) 1180–1186.
[73] L.F. Drummy, B.L. Farmer, R.R. Naik, Correlation of the β-sheet crystal size in silk fibers with the protein amino acid sequence, Soft Matter 3 (2007) 877–882.
[74] Z. Gong, L. Huang, Y. Yang, X. Chen, Z. Shao, Two distinct β-sheet fibrils from silk protein, Chem. Commun. (2009) 7506–7508.
[75] X. Hu, D. Kaplan, P. Cebe, Dynamic protein− water relationships during β-sheet formation, Macromolecules. 41 (2008) 3939–3948.
[76] T. Lefèvre, M.-E. Rousseau, M. Pézolet, Protein secondary structure and orientation in silk as revealed by Raman spectromicroscopy, Biophys. J. 92 (2007) 2885–2895.
[77] L. Liu, X. Yang, H. Yu, C. Ma, J. Yao, Biomimicking the structure of silk fibers via cellulose nanocrystal as β-sheet crystallite, RSC Adv. 4 (2014) 14304–14313.
[78] S. Dinesh Shrivastava, K. Mathai Eldho, P.R. Rajamohanan, T.G. Ajithkumar, K. Vanka, G. Kumaraswamy, Molecular motifs for additives that retard PEO crystallization, Polym. Eng. Sci. 57 (2017) 857–864.
[79] P. Cebe, B.P. Partlow, D.L. Kaplan, A. Wurm, E. Zhuravlev, C. Schick, Using flash DSC for determining the liquid state heat capacity of silk fibroin, Thermochim. Acta 615 (2015) 8–14.
[80] J. Magoshi, S. Nakamura, Studies on physical properties and structure of silk. Glass transition and crystallization of silk fibroin, J. Appl. Polym. Sci. 19 (1975) 1013–1015.
[81] J. Magoshi, Studies on dynamic mechanical properties of drawn silk fibroin, J. Soc. Mater. Sci. Japan. 22 (1973) 499–503.
[82] Q. Lu, X. Hu, X. Wang, J.A. Kluge, S. Lu, P. Cebe, D.L. Kaplan, Water-insoluble silk films with silk I structure, Acta Biomater. 6 (2010) 1380–1387.
[83] I.C. Um, H. Kweon, Y.H. Park, S. Hudson, Structural characteristics and properties of the regenerated silk fibroin prepared from formic acid, Int. J. Biol. Macromol. 29 (2001) 91–97.